Morphological and functional reorganization of rat medial prefrontal cortex in neuropathic pain

Alexia E. Metz[1], Hau-Jie Yau, Maria Virginia Centeno, A. Vania Apkarian, and Marco Martina[2]

Department of Physiology, Northwestern University Feinberg School of Medicine, 303 East Chicago Avenue, Chicago, IL 60611

Edited by Michael M. Merzenich, University of California, San Francisco, CA, and approved December 22, 2008 (received for review October 3, 2008)

Neuropathic pain is a chronic pain that results from lesion or dysfunction of the nervous system. Depression and cognitive decline are often coupled to chronic pain, suggesting the involvement of cortical areas associated with higher cognitive functions. We investigated layer 2/3 pyramidal neurons in acute slices of the contralateral medial prefrontal cortex (mPFC) in the rat spared nerve injury (SNI) model of neuropathic pain and found morphological and functional differences between the mPFC of SNI and sham-operated animals. Basal, but not apical, dendrites of neurons from SNI rats are longer and have more branches than their counterparts in sham-operated animals; spine density is also selectively increased in basal dendrites of neurons from SNI rats; the morphological changes are accompanied by increased contribution to synaptic currents of the NMDA component. Interestingly, the NMDA/AMPA ratio of the synaptic current elicited in mPFC neurons by afferent fiber stimulation shows linear correlation with the rats' tactile threshold in the injured (but not in the contralateral) paw. Our results not only provide evidence that neuropathic pain leads to rearrangement of the mPFC, which may help defining the cellular basis for cognitive impairments associated with chronic pain, but also show pain-associated morphological changes in the cortex at single neuron level.

AMPA | dendrite | mPFC | NMDA | spine

The prefrontal cortex (PFC) is associated with high-order cognitive and emotional functions including attention, decision making, goal-directed behavior, and working memory (1, 2). In humans, different subregions of the PFC have a role in acute pain; the medial prefrontal cortex (mPFC) was found to be involved in signaling the unpleasantness of pain (3); the anterior cingulate cortex mediates the affective component of pain responses (4) and the placebo effect (5); and anticipation of pain is positively correlated with activity in both the anterior cingulate and mPFC (6). Lending support to the hypothesis that chronic pain involves cortical reorganization, functional MRI (fMRI) studies in patients with complex region pain syndrome type I (CRPS-I) and back pain have shown that the patients' real-time rating of perceived intensity of spontaneous pain is associated with novel activity in mPFC (7, 8) when compared with activity patterns that correlate with rating of acute pain stimuli. Additionally, studies in humans with CRPS-I and chronic back pain demonstrate impaired performance on emotional decision-making tasks such as the Iowa Gambling Task (9), which implies involvement of the mPFC. Indeed, the performance of CRPS-I patients resembles that of patients with frontal cortex lesions. In patients with chronic back pain, the extent of activation of the mPFC during spontaneous pain and the extent of emotional, cognitive impairment correlate with the intensity of the pain and the duration of the condition (7). Finally, magnetic resonance studies show that chronic pain is associated with decreased gray matter density in various PFC regions (10, 11). Thus, the emerging picture is that the higher the intensity of chronic back pain the more mPFC is active, which results in worse performance of emotional decision making.

Involvement of prefrontal cortical areas in acute pain perception was first proposed in an article by Fuchs *et al.* (12), and has been well documented in several animal studies; chemical or electrical stimulation of the anterior cingulate cortex has a facilitatory effect on nociceptive heat responses (13). Moreover, overexpression of the NR2B subunit of the NMDA receptor in mouse forebrain resulted in increased sensitivity to inflammatory pain (14) and, conversely, inflammatory pain leads to up-regulation of NR2B subunit expression in the anterior cingulate cortex (15). In line with these findings, a recent study conducted on a rat model of chronic pain showed that injection of D-cycloserine, a partial agonist of the NMDA receptor (16), in mPFC has potent analgesic effect, which is maximum for injections 1–2 mm away from CG1 area and decays at further distance (17).

These results imply that chronic pain disrupts emotional and cognitive functions that are typically associated with the medial prefrontal cortex in primates (the infralimbic cortex of the rat; 18) and suggest that this disruption may involve mPFC reorganization. However, no evidence for morphological or functional changes of mPFC neurons associated with chronic pain has been reported. We show that rat mPFC neurons undergo large morphological and functional changes associated with neuropathic pain and provide evidence of pain-related morphological changes in the cortex.

Results

Patch-clamp recordings and morphological analysis were performed on layer 2/3 pyramidal neurons in the contralateral mPFC of SNI and sham-operated rats 1 week after the surgery.

Tactile thresholds were measured on the day of the experiments. In keeping with a neuropathic pain condition, the von Frey threshold measured on the operated paw was greatly decreased in SNI animals, whereas in sham-operated rats it was very similar to the value measured in control (naïve) animals (threshold values were 0.2 ± 0.02, 2.4 ± 0.15, and 2.0 ± 0.16 g for SNI, sham, and naïve rats, $n = 33$, 28, and 3, respectively).

Only neurons whose morphology was subsequently recovered and were located in layer 2/3 of the cortex of the CG3 and IL areas (distance from dorsal apex $1{,}665 \pm 88$ μm and $1{,}588 \pm 84$ μm for cells from sham and SNI rats, respectively, Fig. 1) were analyzed. Synaptic currents were recorded in CG3 neurons only.

Whole-cell recordings showed that glutamatergic synaptic currents of layer 2/3 pyramidal neurons differ between SNI and sham-operated rats. Excitatory postsynaptic currents (EPSCs) were elicited by stimulation of afferent fibers. For these recordings the extracellular solution contained picrotoxin (50 μM) to block fast GABAergic inhibition and the stimulation electrode was positioned in layer 5. EPSCs were recorded at different

Author contributions: A.V.A. and M.M. designed research; A.E.M., H.-J.Y., M.V.C., and M.M. performed research; A.E.M., H.-J.Y., and M.M. analyzed data; and M.M. wrote the paper.

The authors declare no conflict of interest.

This article is a PNAS Direct Submission.

[1]Present address: Department of Occupational Therapy, University of Toledo, Health Science Campus, 3000 Arlington, Mail Stop 1027, Toledo, OH 43614.

[2]To whom correspondence should be addressed. E-mail: m-martina@northwestern.edu.

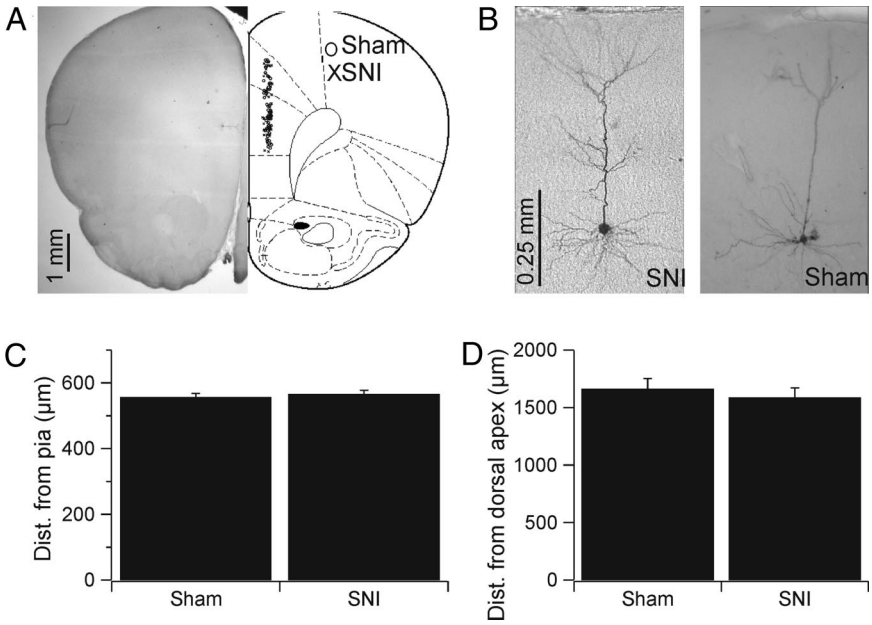

Fig. 1. Topography of the pyramidal neurons investigated. Neurons were patched in slices of the mPFC contralateral to the surgery side. (*A*) A slice containing a biocytin-filled neuron is shown beside a cortical map (adapted from ref. 42). The markers on the map represent the locations of the neurons included in this study (O = cells from sham-operated rats; X = cells from SNI rats). (*B*) Photographs of two representative biocytin-filled neurons, one from a SNI and one from a sham-operated rat. (*C* and *D*) Summary bar charts reporting the topographical coordinates of the neurons included in the study show that the neuronal populations sampled in the two animal groups were overlapping.

membrane potentials (from −90 to +40 mV, 10-mV steps) in control conditions and after blockade of the AMPA component by bath application of 6-cyano-7-nitroquinoxaline-2,3-dione (CNQX) (20 μM). The NMDA/AMPA ratio was then calculated from the peak amplitude of the CNQX-sensitive component measured at −90 mV and the peak amplitude of CNQX-resistant component measured at 40 mV. Analysis of the currents obtained from SNI and sham-operated rats showed that the fraction of current mediated by NMDA channels was significantly larger in SNI animals. The NMDA/AMPA ratio was 0.77 ± 0.1 in SNI and 0.50 ± 0.06 in sham-operated rats (26 and 24 cells, respectively, $P < 0.05$, t test; Fig. 2). Interestingly, a

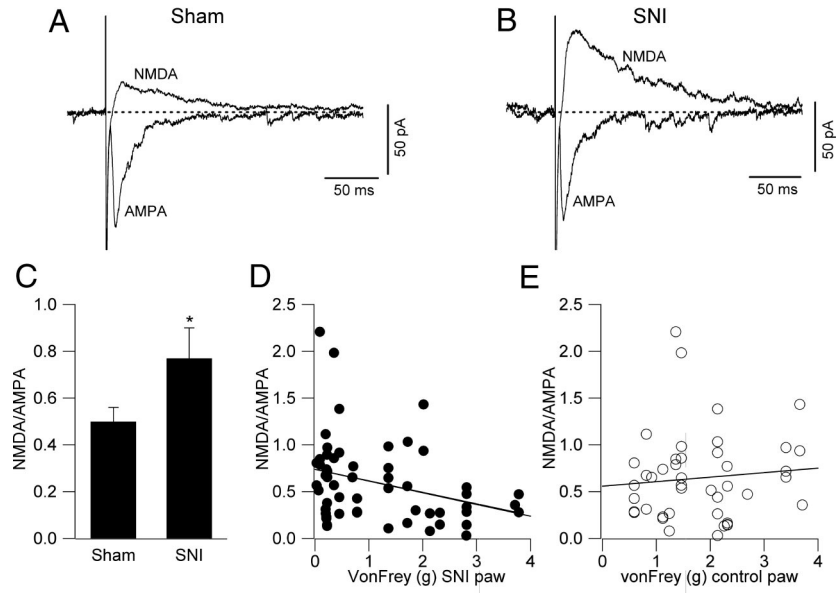

Fig. 2. Increased NMDA/AMPA ratio in SNI mPFC pyramidal cells. (*A* and *B*) Whole-cell recordings in pyramidal neurons from a sham-operated rat (*A*) and a SNI rat (*B*). AMPA currents were recorded at −80 mV. The dotted lines represent the 0 current levels. The AMPA-selective blocker CNQX (20 μM) was then added to the bath solution and CNQX-resistant NMDA currents were recorded at +40 mV. (*C*) Summary of the data obtained from 26 cells of sham-operated and 24 cells of SNI rats. The NMDA/AMPA ratio was 0.5 ± 0.06 in neurons from sham and 0.77 ± 0.1 in cells from SNI animals ($P < 0.05$, two-sided t test). (*D*) Plot of the NMDA/AMPA ratio against tactile threshold measured in the rats' injured paws on the same day of the electrophysiological recordings (data from SNI and sham-operated rats are plotted together). Regression analysis showed a linear correlation between NMDA/AMPA ratio and behavior ($n = 50$, $r = 0.31$, $P < 0.05$). (*E*) Plotting the same data against the tactile threshold in the contralateral paw did not produce any significant correlation ($n = 50$, $r = 0.09$, $P \gg 0.05$).

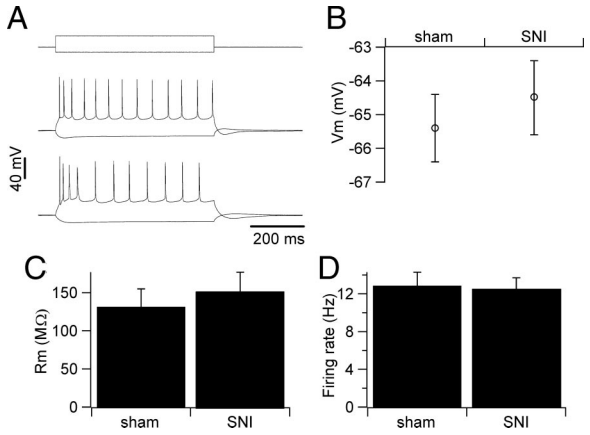

Fig. 3. Basic electrophysiological properties are similar in mPFC pyramidal neurons of sham and SNI rats. One week after the surgery, patch-clamp recordings were obtained from acute slices in the presence of blockers of fast synaptic transmission (3 mM kynurenic acid and 50 μM picrotoxin). (*A*) Current clamp traces obtained in a slice from a sham (upper trace) and a SNI rat in response to injection of hyperpolarizing and depolarizing current pulses. (*B*) Summary plot of the resting membrane potential value in pyramidal cells from the two groups of rats. (*C* and *D*) Bar charts summarizing the value of input resistance and maximum firing rate in cells from the two groups.

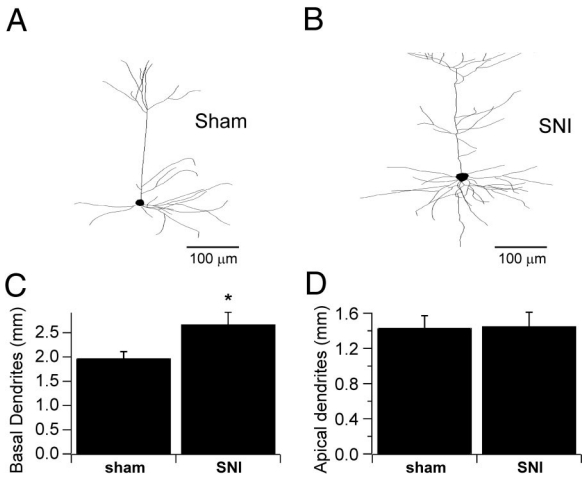

Fig. 4. SNI rat mPFC pyramidal cells have longer basal dendritic arbor. Camera lucida reconstruction of biocytin-filled layer 2/3 mPFC neurons from a sham-operated rat (*A*) and a SNI rat (*B*). (*C* and *D*) Bar charts summarizing the value of total length of the basal (*C*) and apical (*D*) dendrites in 16 cells from sham and 16 cells from SNI rats. The basal dendrite length of neurons from SNI rats was increased by ≈30% ($P < 0.05$).

linear correlation was found between the NMDA/AMPA ratio of the synaptic currents of mPFC pyramidal cells and the rats' tactile threshold (Fig. 2*D*), suggesting that the properties of the synaptic transmission in mPFC have direct consequences on pain perception. Intriguingly, the correlation only existed between the NMDA/AMPA ratio and mechanical threshold in the operated, but not in the contralateral paw (Fig. 2*E*), suggesting that it is associated with allodynia, but not normal tactile perception. In contrast to the synaptic properties, no difference was observed between the two experimental groups with regard to basic electrophysiological properties of layer 2/3 pyramidal neurons. The resting membrane potential, measured in the presence of blockers of fast synaptic transmission (3 mM kynurenic acid and 50 μM picrotoxin, which block ionotropic glutamate and GABAA receptors, respectively), was -65.4 ± 1 mV in sham-operated rats and -64.5 ± 1.1 mV in neurons from SNI rats (Fig. 3; 73 and 90 cells, respectively). Input resistance (132 ± 23 and 152 ± 25 MΩ in sham and SNI neurons, respectively; Fig. 3*C*) and maximum firing rate (12.9 ± 1.4 and 12.6 ± 1.1 Hz in sham and SNI rats, respectively; Fig. 3*D*) on injection of depolarizing current were also similar in animals of the two groups.

Anatomical reconstruction of the filled neurons was performed to study neuronal morphology in pyramidal neurons from the SNI and sham-operated rats. Similar to the electrophysiological recordings, all these experiments were performed in a blinded fashion. A large difference was detected in the length of basal dendrites, which in SNI rats were ≈30% longer than in the sham-operated counterparts (1.96 ± 0.15 mm and 2.54 ± 0.18 mm in dendrites from 16 cells from sham and 16 cells from SNI, $P < 0.05$; Fig. 4*C*). Interestingly, the difference was limited to the basal dendrites, whereas the length of the apical dendrites (obtained summing the length of the trunk to that of the apical branches) was very similar in the two groups (1.43 ± 0.14 mm in sham-operated and 1.45 ± 0.16 mm in SNI animals, 16 cells in each group; Fig. 4*D*).

Our data show that basal dendrites are longer in mPFC pyramidal neurons of SNI animals compared with their sham-operated counterparts. Are these dendrites simply longer, or do they also have more branches? To answer this question, Sholl analysis, a widely used method for quantifying the extent and complexity of neural processes (19), was applied to the dendrites of mPFC pyramidal neurons. This investigation showed that basal dendrites of pyramidal neurons are not only longer but also have more branches in SNI animals. This increased complexity was particularly evident at a distance between 40 and 120 μm from the soma and the difference between neurons from SNI and sham-operated animals peaked at 90 μm from the soma; at this distance, the total number of crossings was ≈40% larger for SNI rats (10.7 ± 0.7 versus 14.6 ± 1.1 crossings in sham-operated and SNI rats, respectively; 16 cells in each group, $P < 0.01$; Fig. 5*A*). In contrast, no significant differences were detected in apical dendrites, similar to what was observed for the dendritic length (the number of crossings was 3.9 ± 0.2 and 3.97 ± 0.2 in sham and SNI rats, respectively, 16 cells in each group; Fig. 5*B*). Thus, cingulate pyramidal neurons of SNI rats undergo selective morphological rearrangement of the basal dendrites, which become longer and more complex.

The observed changes in the properties of the synaptic currents and the spatial selectivity of the observed morphological

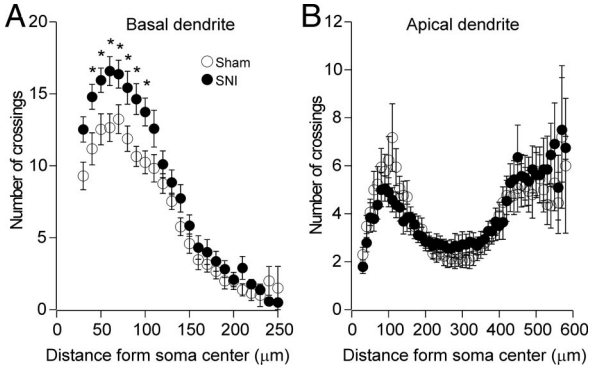

Fig. 5. Basal dendrites of cells from SNI rats are more complex. (*A*) Sholl analysis of basal dendrites of layer 2/3 mPFC pyramidal neurons from sham-operated (hollow symbols, 16 cells) and SNI (filled symbols, 16 cells) rats. Note that the large difference between the number of crossings in neurons from SNI and sham-operated rats at each point between 40 and 100 μm from the soma. (*B*) Similar analysis in apical dendrites (16 cells in each group) failed to detect significant differences at any distance from the soma. (*, $P < 0.05$, ANOVA for repeated measures).

NEUROSCIENCE

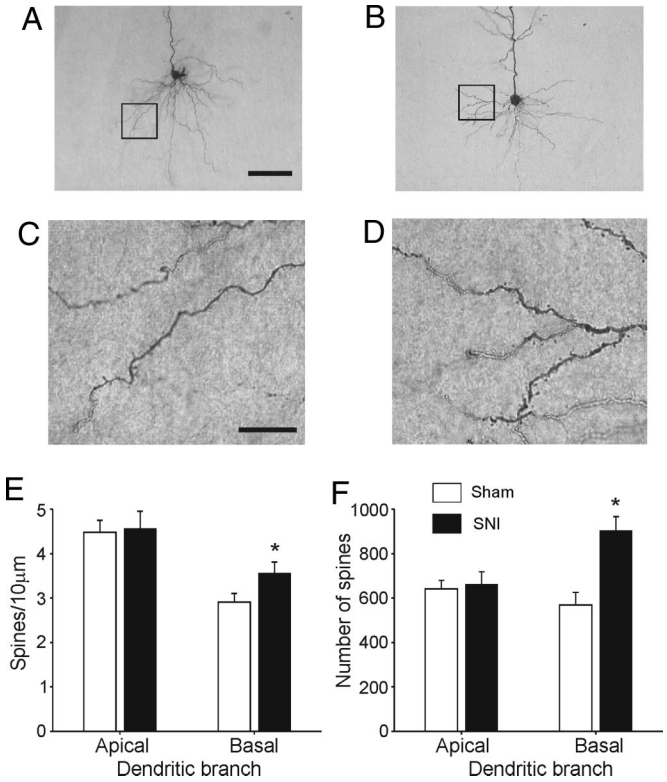

Fig. 6. Spine density is increased in basal dendrites of SNI neurons. (*A* and *B*) Photographs of a mPFC pyramidal neuron from a sham-operated rat (*A*) and a SNI rat (*B*). (Scale bar, 100 μm.) Dendritic segments included in the boxed areas are shown at higher magnification in *C* and *D*. (Scale bar, 20 μm.) (*E*) Bar chart of the spine density in apical and basal dendrites of pyramidal cells from sham operated (open columns) and SNI rats (filled columns). (*F*) Total number of spines, extrapolated from spine density and dendritic length, in apical and basal dendrites of neurons from sham-operated and SNI rats (*, $P < 0.05$).

changes may suggest that the alterations in dendritic morphology are related to selected neuronal inputs. Most of the excitatory synaptic contacts on pyramidal neurons are localized on spines. We explored the possibility that morphological reorganization also produces alterations in spine density. Spines (operationally identified as structures with both head and neck; see *Methods*) were counted over basal and apical dendrites of prefrontal cortical neurons (Fig. 6). Whereas no differences were observed in spine density on the apical dendrites (4.5 ± 0.27 and 4.6 ± 0.38 spines per 10 μm for cells from sham and SNI animals, $n = 26$ and 23, respectively), the basal dendrite spine density in SNI neurons was increased by $\approx$25% compared with sham-operated animals (2.9 ± 0.2 versus 3.6 ± 0.25 spines per 10 μm in dendrites from 26 control neurons and 23 SNI neurons, respectively, $P < 0.05$; Fig. 6*E*). This pattern was similar to that observed in SNI neurons for dendritic length which also showed a significant increase that was restricted to basal dendrites only. If both dendritic length and spine density are taken into account, the extrapolated number of excitatory contacts to the basal dendrites of mPFC neurons of SNI animals is increased by $\approx$60% compared with sham-operated animals (Fig. 6*F*).

Discussion

We performed patch-clamp recordings and anatomical analysis of layer 2/3 pyramidal neurons in the contralateral medial prefrontal cortex of SNI and sham-operated rats. We found that neuropathic pain is associated with morphological and functional changes. Morphologically, neurons from SNI animals showed increased dendritic complexity and spine density in basal dendrites compared with the sham-operated group; functionally, SNI neurons showed a large increase in the NMDA/AMPA ratio in currents synaptically evoked by layer 5 stimulation, whereas the basic electrical properties of the neurons did not differ between the two groups.

Pain-Associated Neuronal Reorganization. Neurochemical and morphological rearrangement of the spinal cord are well known to be present in animal models of chronic pain (20–23) and functional changes have been previously described in association with pain in primary somatosensory cortex (24) as well as in the anterior cingulate cortex, where up-regulation of NMDA NR2B subunits after peripheral inflammation has been recently shown (15). To our knowledge, however, morphological changes associated with pain have been described. Our data suggest that the mPFC undergoes profound reorganization, both morphological and functional, associated with neuropathic pain.

Further support to the idea of a major involvement of the mPFC in the neurophysiological processes of chronic pain perception was recently presented by Millecamps *et al.* (17). These authors used the SNI model, the same model of neuropathic pain used in this article, to test the antinociceptive potential of D-cycloserine, an NMDA partial agonist. Interestingly, they found that the effect of acute cortical infusion of the drug was highly correlated with the infusion site and that the maximum effect was observed in the prelimbic cortex, within 2 mm ventrally from CG1, which is the same area described in this article. Thus, multiple approaches suggest an important role of the mPFC in the perception of chronic pain. Another interesting point concerns the temporal window of the observed morphological changes. Our observations were performed 6–8 days after the onset of pain (the SNI surgery). This implies that morphological changes appear rapidly after the injury. These data are reminiscent of the increase in NR2B subunits described in the cingulate cortex of mice exposed to inflammatory pain (15). In that case, NR2B expression increase became evident already at 1 day, and remained elevated at 1 week. It will be important, in future experiments, to establish whether the observed spine density change is also accompanied by altered NMDA subunit expression, whether their temporal time courses match, and whether or not these changes are reversible.

What Are the Circuits Affected by Neuropathic Pain? The changes described in this article are located in the mPFC, a brain area deeply involved in higher cognitive functions (25, 26). What pathways could be involved? The observed morphological changes were limited to the basal dendrites; this suggests a pathway-specific phenomenon. Basal dendrites of layer 2/3 neurons receive inputs from other layer 2/3 pyramidal neurons and from deeper cortical layers (27–29). Thus, morphological changes of basal dendrites may suggest reorganization of intracortical circuits more than changes related to the reorganization of extracortical inputs, which may depend on the surgical deafferentation.

At the same time it is known that projections from the basolateral nucleus of the amygdala (BLA) to the mPFC form a neural circuit that has been implicated in a number of cognitive and emotional processes, such as the acquisition and extinction of conditioned fear (30) and different forms of decision making (31). Such anatomical connectivity appears to lay the ground for understanding the impaired performance on an emotional decision-making task observed in patients with chronic pain (9). It is worth noting that in the medial prefrontal cortex the BLA inputs converge with dopamine input from the ventral tegmental area (VTA), forming a neural circuit implicated in certain cognitive and emotional processes. It has been shown that the dopamine afferents to the mPFC form synaptic contacts almost exclusively with dendritic spines (32), thus the increased spine

density might mediate inputs from this afferent pathway. In keeping with these observations, abnormal dopamine response has been observed in chronic pain conditions such as fibromyalgia (33).

The medial prefrontal cortex, and the Cg3 area in particular, also receives afferents from the hippocampus (34, 35). Interestingly, limbic nuclei and the hippocampus express markers of neuronal activation, such as immediate early genes (in particular c-Fos), in response to peripheral noxious stimulation (36). Moreover, the hippocampal afferents to the mPFC appear intriguing when considering the hippocampal role in memory encoding (reviewed in refs. 37 and 38). The coexistence of afferents from the amygdala and the hippocampus may suggest an anatomical complement to the term "pain memory" that is being used to describe neuropathic pain (39). Further studies addressing the reorganization of local cortical maps will be necessary to establish which circuits are involved. In this context, it is worth noticing that a recent article (40) shows that pharmacological inactivation of the same mPFC area as the one investigated in our study results in marked reduction of learned behavioral selection.

A final consideration concerns the relation between the data presented here and data in human chronic pain patients in which atrophy of the dorsolateral prefrontal cortex has been reported (10). In rats, the mPFC consists of four main divisions, which from dorsal to ventral are the medial agranular, anterior cingulate, prelimbic, and infralimbic cortex (reviewed in ref. 18). Although the dorsal regions of mPFC (such as the cingulate cortex) appear involved in motor behaviors, more ventral regions of mPFC are associated with diverse emotional, cognitive, and mnemonic processes. It has been suggested that the rat infralimbic cortex is functionally homologous to the orbitomedial cortex of primates whereas the prelimbic and the ventral anterior cingulate cortices are homologous to the dorsolateral cortex of primates (18). Thus, the rat prelimbic area (that was examined in this study) may be considered the functional homologous of the human dorsolateral PFC. It is therefore intriguing to suggest that the increased spine number and NMDA currents may lead to increased glutamatergic input-mediated calcium influx, which, in turn, may result into glutamate excitotoxicity and neuronal loss.

Methods

Spared Nerve Injury (SNI) Model: Surgery. Twenty- to 21-day-old rats were anesthetized by using gas anesthesia (isoflurane 1–2%, and 30% N_2O, 70% O_2). For induction of SNI neuropathy, the left sciatic nerves were exposed at the level of the trifurcation into the sural, tibial, and common peroneal nerves. The tibial and common peroneal nerves were tightly ligated and severed, leaving the sural nerve intact. A second group of animals was used for control sham surgery. In this case, the left sciatic nerve was exposed just as in the SNI procedure but was not further manipulated.

Behavioral Test for Tactile Sensitivity. Tactile sensitivity of the spared region of the operated paws was measured from the withdrawal responses to mechanical stimulation with von Frey filaments. Animals were placed in a cage with wire grid floor and allowed to habituate to the environment for 15 min. Filaments (Stoelting) of varying forces were applied to the plantar surface of the hind paw in ascending order. Each filament was applied for a maximum of 10 s. Paw withdrawal during the application was considered a positive response. Fifty percent response thresholds were calculated according to Chaplan *et al.* (41).

Patch Clamp in Cortical Brain Slices. All of the experiments were performed in a blinded fashion (the experimenter did not know whether the brain was from a sham or SNI rat). Six to eight days after the surgery rats were deeply anesthetized with isoflurane and decapitated. The brains were quickly removed from the skull in ice-cold modified artificial cerebrospinal fluid (ACSF), containing (in mM): 125 NaCl, 25 $NaHCO_3$, 2.5 KCl, 1.25 NaH_2PO_4, 0.5 $CaCl_2$, 7 $MgCl_2$, and 25 glucose, bubbled with 95% O_2 and 5% CO_2. Coronal slices (300 μm thick) of the prefrontal cortex were cut by using a tissue slicer (Dosaka) and then stored in sucrose-rich ACSF (in mM: 87 NaCl, 25 $NaHCO_3$, 2.5 KCl, 1.25 NaH_2PO_4, 0.5 $CaCl_2$, 7 $MgCl_2$, 75 sucrose, and 25 glucose, bubbled with 95% O_2 and 5% CO_2) for 30 min at 35 °C and subsequently at room temperature. For recordings, slices were transferred to the recording chamber and continuously superfused with ACSF (in mM: 125 NaCl, 25 $NaHCO_3$, 2.5 KCl, 1.25 NaH_2PO_4, 1.2 $CaCl_2$, 1 $MgCl_2$, and 25 glucose, bubbled with 95% O_2 and 5% CO_2). Layer 2/3 pyramidal neurons of the mPFC contralateral to the surgery side of SNI and sham animals were selected by using infrared differential interference videomicroscopy on the basis of location, shape, and size. Patched neurons were filled with biocytin (or, in a subset of cells, with Alexa Fluor 594) and subsequently histologically visualized. Only neurons that could be subsequently identified and confirmed to be in layer 2/3 of the CG3 and IL areas were analyzed. The populations of SNI and sham neurons were spatially homogeneous: the distance from dorsal apex was 1,665 $\pm$ 88 μm and 1,588 $\pm$ 84 μm for cells from sham and SNI rats, respectively.

Recordings were performed by using an Axoptach 200B amplifier. Pipettes were pulled from borosilicate glass (Garner) and had tip resistance in working solution of 2–5 MΩ. Series resistances were $\leq$25 MΩ and were 75–80% compensated. The intrapipette solution contained 140 mM K-gluconate, 8 mM NaCl, 2 mM $MgCl_2$, 2 mM Na_2ATP, 0.3 mM GTP, 1 mM EGTA, 10 mM Hepes, and biocytin (1.5 mg/mL) (pH 7.2 with KOH). In synaptic stimulation experiments, 50 μM picrotoxin and 1 μM glycine were included in the bath solution, and 5 mM QX314 was included in the internal solution—cells recorded in these conditions were not included in analysis of intrinsic properties. The resting membrane potential was recorded immediately on gaining whole-cell access. Input resistance was calculated as the slope of a V-I plot, measuring the peak voltage change resulting from a series of 1-s current injections from $-$200 to $+$40 pA. The firing rate was defined as the number of spikes evoked with 1-s injections of depolarizing current of increasing amplitudes. A response was considered saturating when the spikes after the first did not overshoot (their peak did not cross the 0 mV line) because of sodium channel inactivation.

Synaptic currents were elicited by electrical stimulation of the afferent fibers; this was obtained by using a large patch pipette ($\approx$1 MΩ) filled with Hepes-buffered ACSF (pH 7.4) placed in layer 5 (15). EPSCs were evoked by extracellular stimulation by using a 200-μs-long pulse delivered with an isolation unit (A360 WPI). Stimuli (80–160 μA) were delivered at 0.1 Hz. The amplitude of each EPSC was measured relative to a 40-ms-long baseline period starting 1 ms before stimulation. All recordings were performed at 23–25 °C.

Chemicals and drugs were from Sigma. Picrotoxin and kynurenic acid stock solutions (50 mM and 1 M, respectively) were stored at 2–4 °C and working solutions were prepared freshly every day.

Anatomical Visualization of Patched Cells. Biocytin-filled (1.5 mg/mL) cells were processed by using a standard 3,3′-diaminobenzidine (DAB) staining protocol. At the end of the recording slices were fixed in 4% paraformaldehyde in 0.1 M phosphate buffer (PB, pH 7.4) for a minimum of 24 h, at 4 °C. After fixation slices were rinsed in PB and subsequently treated with hydrogen peroxide (1%, 20–30 min) and the slices were permeabilized in a solution of 2% Triton X-100 for 1 h. The slices were then incubated in PB containing 1% avidin-biotinylated horseradish peroxidase complex (ABC, Vector Laboratories) for 2 h at 4 °C. Excess ABC was removed by 4 rinses in PB. Slices were developed with 0.1% DAB and then embedded in Mowiol (Aldrich) to be examined by bright field light microscopy. Cell location was quantified in 2 axes: the distance from the most dorsal point of the midline between the 2 cerebral hemispheres (dorsal apex) was measured to produce a *y* axis value and the depth from pia was measured orthogonally from the midline producing an *x* axis value (Fig. 1).

Dendritic Morphology. Cells were digitally reconstructed in 3 dimensions by using NeuroLucida software at 20$\times$ and 40$\times$ magnification. Dendritic length and branch patterns were analyzed by using applications within NeuroExplorer (Microbrightfield).

All of the cells included in the analysis were located in the dorsomedial mPFC (CG3, IL; see ref. 44); the distance from the pial surface was almost identical for the two groups; it was 559 $\pm$ 14 μm and 566 $\pm$ 13 μm for cells from sham and SNI rats, respectively; the distance from the dorsal apex of the midline was 1,665 $\pm$ 88 μm and 1,588 $\pm$ 84 μm for cells from sham and SNI rats, respectively. Only cells in which the filling was optimal in both apical and basal dendrites and in which no major branches appeared to have been cut during the slicing procedure were used for anatomical analysis. Electrophysiological recordings, anatomical measurements, and analyses were all performed in a blinded fashion. Data are reported as mean $\pm$ SEM; statistical significance was set at $P < 0.05$ (* in figures) and determined by using two-tailed *t* tests or ANOVA for repeated measures, as appropriate.

Spine Counting. Light microscope and high magnification oil immersion objectives (63×, 1.4 NA, Zeiss) were used to count the number of dendritic spines. Distances were measured linearly by using NeuroLucida (Microbrightfield). For each neuron, counting was performed on a 50- to 100-μm segment of the principal apical dendrite (the proximal end of this segment was never closer than 50 μm from the center of the soma), a 30-μm segment of secondary apical dendrite, and two segments (each at least 15 μm long) of basal dendrite (the proximal endings of these segments were at least 20 μm from the soma); the number of spines on the selected segments was manually counted at 63× through the microscope oculars (10×). Spines were counted only if they had both a punctuate head and visible neck. A subset of neurons was counted by two different investigators to ensure consistency of counting. No significant differences were found when the same segment was counted by different investigators.

ACKNOWLEDGMENTS. We thank Lisa J. Carroll for help with the analysis of morphological data, Dr. M. Millecamps for help in the early phase of the project, and Dr. E. Mugnaini for helpful discussions. This work was supported in part by a National Alliance for Research on Schizophrenia and Depression Young Investigator Award (M.M.), the Epilepsy Foundation (M.M.), and National Institutes of Health Grant NS 57704 (to A.V.A.).

1. Gusnard DA, Akbudak E, Shulman GL, Raichle ME (2001) Medial prefrontal cortex and self-referential mental activity: relation to a default mode of brain function. *Proc Natl Acad Sci USA* 98:4259–4264.
2. Phelps EA, Delgado MR, Nearing KI, LeDoux JE (2004) Extinction learning in humans: role of the amygdala and vmPFC. *Neuron* 43:897–905.
3. Lorenz J, *et al.* (2002) A unique representation of heat allodynia in the human brain. *Neuron* 35:383–393.
4. Rainville P, Duncan GH, Price DD, Carrier B, Bushnell MC (1997) Pain affect encoded in human anterior cingulate but not somatosensory cortex. *Science* 277:968–971.
5. Wager TD, *et al.* (2004) Placebo-induced changes in FMRI in the anticipation and experience of pain. *Science* 303:1162–1167.
6. Porro CA, *et al.* (2002) Does anticipation of pain affect cortical nociceptive systems? *J Neurosci* 22:3206–3214.
7. Baliki MN, *et al.* (2006) Chronic pain and the emotional brain: Specific brain activity associated with spontaneous fluctuations of intensity of chronic back pain. *J Neurosci* 26:12165–12173.
8. Schweinhardt P, *et al.* (2008) Investigation into the neural correlates of emotional augmentation of clinical pain. *Neuroimage* 40:759–766.
9. Apkarian AV, *et al.* (2004) Chronic pain patients are impaired on an emotional decision-making task. *Pain* 108:129–136.
10. Apkarian AV, *et al.* (2004) Chronic back pain is associated with decreased prefrontal and thalamic gray matter density. *J Neurosci* 24:10410–10415.
11. Kuchinad A, *et al.* (2007) Accelerated brain gray matter loss in fibromyalgia patients: premature aging of the brain? *J Neurosci* 27:4004–4007.
12. Fuchs PN, Balinsky M, Melzack R (1996) Electrical stimulation of the cingulum bundle and surrounding cortical tissue reduces formalin-test pain in the rat. *Brain Res* 743:116–123.
13. Calejesan AA, Kim SJ, Zhuo M (2000) Descending facilitatory modulation of a behavioral nociceptive response by stimulation in the adult rat anterior cingulate cortex. *Eur J Pain* 4:83–96.
14. Wei F, *et al.* (2001) Genetic enhancement of inflammatory pain by forebrain NR2B overexpression. *Nat Neurosci* 4:164–169.
15. Wu LJ, *et al.* (2005) Upregulation of forebrain NMDA NR2B receptors contributes to behavioral sensitization after inflammation. *J Neurosci* 25:11107–11116.
16. Hood WF, Compton RP, Monahan JB (1989) D-cycloserine: A ligand for the N-methyl-D-aspartate coupled glycine receptor has partial agonist characteristics. *Neurosci Lett* 98:91–95.
17. Millecamps M, *et al.* (2007) D-cycloserine reduces neuropathic pain behavior through limbic NMDA-mediated circuitry. *Pain* 132:108–123.
18. Vertes RP (2006) Interactions among the medial prefrontal cortex, hippocampus and midline thalamus in emotional and cognitive processing in the rat. *Neuroscience* 142:1–20.
19. Sholl DA (1953), Dendritic organization in the neurons of the visual and motor cortices of the cat. *J Anat* 87:387–406.
20. Abbadie C, Trafton J, Liu H, Mantyh PW, Basbaum AI (1997) Inflammation increases the distribution of dorsal horn neurons that internalize the neurokinin-1 receptor in response to noxious and non-noxious stimulation. *J Neurosci* 17:8049–8060.
21. Goff JR, Burkey AR, Goff DJ, Jasmin L (1998) Reorganization of the spinal dorsal horn in models of chronic pain: Correlation with behaviour. *Neuroscience* 82:559–574.
22. Schwei MJ, *et al.* (1999) Neurochemical and cellular reorganization of the spinal cord in a murine model of bone cancer pain. *J Neurosci* 19:10886–10897.
23. Basbaum AI (1999) Spinal mechanisms of acute and persistent pain. *Reg Anesth Pain Med* 24:59–67.
24. Maihöfner C, Handwerker HO, Neundörfer B, Birklein F (2003) Patterns of cortical reorganization in complex regional pain syndrome. *Neurology* 61:1707–1715.
25. Walton ME, Bannerman DM, Rushworth MF (2002) The role of rat medial frontal cortex in effort-based decision making. *J Neurosci* 22:10996–11003.
26. Saxe R (2006) Uniquely human social cognition. *Curr Opin Neurobiol* 16:235–239.
27. Shepherd GM, Svoboda K (2005) Laminar and columnar organization of ascending excitatory projections to layer 2/3 pyramidal neurons in rat barrel cortex. *J Neurosci* 25:5670–5679.
28. Larkum ME, Waters J, Sakmann B, Helmchen F (2007) Dendritic spikes in apical dendrites of neocortical layer 2/3 pyramidal neurons. *J Neurosci* 27:8999–9008.
29. Weiler N, Wood L, Yu J, Solla SA, Shepherd GM (2008) Top-down laminar organization of the excitatory network in motor cortex. *Nat Neurosci* 11:360–366.
30. Maren S, Quirk GJ (2004) Neuronal signalling of fear memory. *Nat Rev Neurosci* 5:844–852.
31. Bechara A, Damasio H, Damasio AR, Lee GP (1999) Different contributions of the human amygdala and ventromedial prefrontal cortex to decision-making. *J Neurosci* 19:5473–5481.
32. Bacon SJ, Headlam AJ, Gabbott PL, Smith AD (1996) Amygdala input to medial prefrontal cortex (mPFC) in the rat: A light and electron microscope study. *Brain Res* 720:211–219.
33. Wood PB, *et al.* (2007) Fibromyalgia patients show an abnormal dopamine response to pain. *Eur J Neurosci* 25:3576–3582.
34. Hoover WB, Vertes RP (2007) Anatomical analysis of afferent projections to the medial prefrontal cortex in the rat. *Brain Struct Funct* 212:149–179.
35. Zeng D, Stuesse SL (1991) Morphological heterogeneity within the cingulate cortex in rat: a horseradish peroxidase transport study. *Brain Res* 565:290–300.
36. Aloisi AM, Zimmermann M, Herdegen T (1997) Sex-dependent effects of formalin and restraint on c-Fos expression in the septum and hippocampus of the rat. *Neuroscience* 81:951–958.
37. Moser MB, Moser EI (1998) Functional differentiation in the hippocampus. *Hippocampus* 8:608–619.
38. Shapiro ML, Eichenbaum H (1999) Hippocampus as a memory map: Synaptic plasticity and memory encoding by hippocampal neurons. *Hippocampus* 9:365–384.
39. Zimmermann M (2001) Pathobiology of neuropathic pain. *Eur J Pharmacol* 429:23–37.
40. Ishikawa A, Ambroggi F, Nicola SM, Fields HL (2008) Dorsomedial prefrontal cortex contribution to behavioral and nucleus accumbens neuronal responses to incentive cues. *J Neurosci* 28:5088–5098.
41. Chaplan SR, Bach FW, Pogrel JW, Chung JM, Yaksh TL (1994) Quantitative assessment of tactile allodynia in the rat paw. *J Neurosci Methods* 53:55–63.
42. Paxinos G, Watson C (1998) *The Rat Brain in Stereotaxic Coordinates* (Academic, San Diego).